Inorganic Chemistry

ARTICLE

pubs.acs.org/IC

Magnetic Exchange Interactions and Magneto-Structural Correlations in Heterobridged μ-Phenoxo-$\mu_{1,1}$-Azide Dinickel(II) Compounds: A Combined Experimental and Theoretical Exploration

Sujit Sasmal,[†] Susanta Hazra,[†] Parimal Kundu,[‡] Supriya Dutta,[§] Gopalan Rajaraman,*[,∥] E. Carolina Sañudo,*[,⊥] and Sasankasekhar Mohanta*[,†]

[†] Department of Chemistry, University of Calcutta, 92 A. P. C. Road, Kolkata 700 009, India

[‡] Department of Chemistry, Maharaja Manindra Chandra College, 20 Ramkanto Bose Street, Kolkata 700 003, India

[§] Department of Inorganic Chemistry, Indian Association for the Cultivation of Science, Kolkata 700 032, India

[∥] Department of Chemistry, Indian Institute of Technology Bombay, Powai, Mumbai 400 076, India

[⊥] Department de Química Inorgànica i Institut de Nanociència i Nanotecnologia, Universitat de Barcelona, Diagonal 647, 08028 Barcelona, Spain

Supporting Information

ABSTRACT: This investigation presents the syntheses, crystal structures, magnetic properties, and density functional theoretical modeling of magnetic behavior of two heterobridged μ-phenoxo-$\mu_{1,1}$-azido dinickel(II) compounds $[Ni^{II}_2(L^1)_2(\mu_{1,1}\text{-}N_3)(N_3)(H_2O)]\cdot CH_3CH_2OH$ (**1**) and $[Ni^{II}_2(L^2)_2(\mu_{1,1}\text{-}N_3)(CH_3CN)(H_2O)](ClO_4)\cdot H_2O\cdot CH_3CN$ (**2**), where HL^1 and HL^2 are the [1 + 1] condensation products of 3-methoxysalicylaldehyde and 1-(2-aminoethyl)-piperidine (for HL^1)/4-(2-aminoethyl)-morpholine (for HL^2), along with density functional theoretical magneto-structural correlations of μ-phenoxo-$\mu_{1,1}$-azido dinickel(II) systems. Compounds **1** and **2** crystallize in orthorhombic (space group *Pbca*) and monoclinic (space group $P2_1/c$) systems, respectively. The coordination environments of both metal centers are distorted octahedral. The variable-temperature (2−300 K) magnetic susceptibilities at 0.7 T of both compounds have been measured. The interaction between the metal centers is moderately ferromagnetic; $J = 16.6$ cm^{-1}, $g = 2.2$, and $D = -7.3$ cm^{-1} for **1** and $J = 16.92$ cm^{-1}, $g = 2.2$, and D(Ni1) = D(Ni2) = −6.41 cm^{-1} for **2**. Broken symmetry density functional calculations of exchange interaction have been performed on complexes **1** and **2** and provide a good numerical estimate of J values (15.8 cm^{-1} for **1** and 15.35 cm^{-1} for **2**) compared to experiments. The role of Ni−N bond length asymmetry on the magnetic coupling has been noted by comparing the structures and J values of complexes **1** and **2** together with previously published dimers **3** (*Eur. J. Inorg. Chem.* **2009**, 4982), **4** (*Inorg. Chem.* **2004**, *43*, 2427), and **5** (*Dalton Trans.* **2008**, 6539). Our extensive DFT calculations reveal an important clue to the mechanism of coupling where the orientation of the magnetic orbitals seems to differ with asymmetry in the Ni−N bond lengths. This difference in orientation leads to a large change in the overlap integral between the magnetic orbitals and thus the magnetic coupling. DFT calculations have also been extended to develop several magneto-structural correlations in this type of complexes and the correlation aim to focus on the asymmetry of the Ni−N bond lengths reveal that the asymmetry plays a proactive role in governing the magnitude of the coupling. From a completely symmetric Ni−N bond length, two behaviors have been noted: with a decrease in bond length there is an increase in the ferromagnetic coupling, while an increase in the bond lengths leads to a decrease in ferromagnetic interaction. The later correlation is supported by experiments. The magnetic properties of **1**, **2**, and three previously reported related compounds have been discussed in light of the structural parameters and also in light of the theoretical correlations determined here.

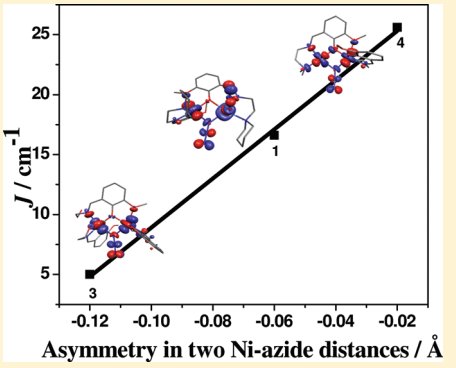

INTRODUCTION

Major aspects of the interdisciplinary frontier research area of molecular magnetism are understanding the mechanism of the spin coupling and determination of magneto-structural correlations,[1−4] from the studies of discrete molecules, and utilization of derived ideas in large clusters or extended systems to get molecule-based magnetic materials.[5−7] The most important systems to explore fundamental aspects are discrete dinuclear exchange-coupled metal complexes because they make possible the evaluation of the pairwise exchange interactions, which can in turn be used to qualitatively assess the coupling in higher nuclearity systems; in fact, most of the experimental or theoretical magneto-structural correlations have been established from the studies of dinuclear compounds.[1,2]

Received: April 21, 2011
Published: June 23, 2011

The nature and magnitude of the magnetic exchange interaction in heterobridged exchange-coupled compounds are governed by the structural and electronic behavior of different types of bridges.[1a,2d,8−15] Magnetic studies of heterobridged dicopper(II) compounds having μ-hydroxo/alkoxo/phenoxo-μ-X (X = azide, thiocyanate, cyanate, pyrazolate, carboxylate, 7-azaindolate, etc.) bridging moieties have been much investigated, and the origin of exchange interactions therein have been well explained on the basis of orbital complementarity and orbital counter-complementarity effects.[1a,8] In contrast, magnetic properties of heterobridged compounds of other 3d metal ions have been much less investigated.[9−15] Again, most of these heterobridged compounds of 3d metal ions, other than of copper(II), are polynuclear, and therefore, evaluation of the exchange integral for a particular heterobridged moiety is not always possible.[13−15] Clearly, design and magnetic studies of discrete heterobridged complexes of 3d metal ions, other than of copper(II), deserve importance.

The theoretical tools play an important role in the field of molecular magnetism to reproduce, analyze, and predict the magnetic properties of compounds of interest.[3,4,16−18] Developing magneto-structural correlations is a challenging task for experimentalist as selecting the unique structural parameter on which the magnetic properties are strongly correlated requires a large number of complexes possessing similar structural topology. On the other hand, such correlations can be easily developed and the trend can be analyzed using computational tools.[4] Due to the complex mechanism which operates in heterobridged dinuclear systems and the presence of cooperativity among dissimilar bridges, developing magneto-structural correlations on heterobridged dinuclear compounds is an intricate task.

We observed previously that the Schiff base ligands obtained on condensation of 3-methoxysalicylaldehyde with an amine having another potential donor center, ethanolamine, for example, stabilize heterobridged dinickel(II) complexes if an inorganic bridging ligand, azide, cyanate, etc., be also utilized in synthesis.[2d,9] These heterobridged μ-phenoxo-$\mu_{1,1}$-NCO/N_3 dinickel(II) compounds exhibit ferromagnetic interaction, indicating that such organic ligands may be used for designed synthesis of ferromagnetically coupled compounds. Interestingly, a unique example of bridge distance dependency of the exchange interaction has emerged from the magnetic properties of the μ-phenoxo-$\mu_{1,1}$-N_3 dinickel(II) compound,[2d] and therefore, we have been more interested in both experimental and density functional theoretical studies of μ-phenoxo-$\mu_{1,1}$-N_3 dinickel(II) compounds with the expectation to get more insight on the structure−property correlation. We anticipated from our previous studies that other ligands which are similar to 3-methoxysalicylaldehyde−ethanolamine would stabilize μ-phenoxo-$\mu_{1,1}$-N_3 dinickel(II) systems. Accordingly, on changing the amine counterpart of the ligand from ethanolamine to 1-(2-aminoethyl)-piperidine (for HL^1; Scheme 1)/4-(2-aminoethyl)-morpholine (for HL^2; Scheme 1), we prepared two μ-phenoxo-$\mu_{1,1}$-N_3 dinickel(II) compounds $[Ni^{II}_2(L^1)_2(\mu_{1,1}\text{-}N_3)(N_3)(H_2O)]\cdot CH_3CH_2OH$ (**1**) and $[Ni^{II}_2(L^2)_2(\mu_{1,1}\text{-}N_3)(CH_3CN)(H_2O)](ClO_4)\cdot H_2O\cdot CH_3CN$ (**2**). Herein, we report the syntheses, crystal structures, and observed magnetic properties of **1** and **2**, DFT modeling of magnetic behavior of **1**, **2**, and previously reported μ-phenoxo-$\mu_{1,1}$-N_3 dinickel(II) compounds, along with interesting density functional theoretical magneto-structural correlations demonstrating the dependency of the exchange integral on bond distances and angles of both bridging groups as well as on the asymmetry in the two Ni−N(azide) bond lengths.

Scheme 1. Chemical Structures of HL^1 and HL^2

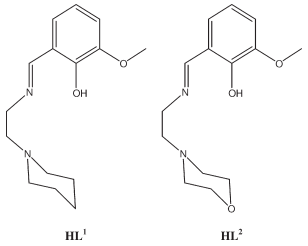

EXPERIMENTAL SECTION

Materials and Physical Measurements. All reagents and solvents were purchased from commercial sources and used as received. Elemental (C, H, and N) analyses were performed on a Perkin-Elmer 2400 II analyzer. IR spectra were recorded in the region 400−4000 cm^{-1} on a Bruker-Optics Alpha-T spectrophotometer with samples as KBr disks. Variable-temperature magnetic susceptibility and magnetization measurements were carried out with a Quantum Design MPMS SQUID magnetometer. Diamagnetic corrections were estimated from the Pascal constants.

Computational Details. There has been a great deal of interest in the evaluation of magnetic exchange couplings using the techniques of quantum chemistry.[19] For very large systems the most widely used scheme is Noodleman's broken symmetry (BS) approach, derived from a spin-unrestricted reference wave function.[20] The Noodleman's BS approach along with the widely used exchange-correlation functional, B3LYP, provide a good numerical estimate of the exchange coupling constant compared to experiment.[18,21,22] Accordingly, all calculations here have used the B3LYP[23] functional with the valence triple-ζ quality basis sets (TZV) of Ahlrichs and co-workers.[24] All calculations were performed using the GAUSSIAN 03 suite of programs[25] with an initial guess made using Jaguar 7.0. There are many approaches to compute the exchange interactions from the broken symmetry energies, and here, we adopted the pairwise interaction model to compute the exchange coupling as the chosen computational setup together with this model yields a good estimate of the coupling constants in many dinuclear as well as polynuclear complexes.[17a,21]

Syntheses of $[Ni^{II}_2(L^1)_2(\mu_{1,1}\text{-}N_3)(N_3)(H_2O)]\cdot CH_3CH_2OH$ (1) and $[Ni^{II}_2(L^2)_2(\mu_{1,1}\text{-}N_3)(CH_3CN)(H_2O)](ClO_4)\cdot H_2O\cdot CH_3CN$ (2). These two compounds were prepared following a similar procedure to that described below for **1**, except that 4-(2-aminoethyl)-morpholine and acetonitrile were used for **2** instead of 1-(2-aminoethyl)-piperidine and ethanol, respectively, for **1**.

A methanol (10 mL) solution of 1-(2-aminoethyl)-piperidine (0.128 g, 1 mmol) was added to a methanol solution (20 mL) of 3-methoxysalicylaldehyde (0.152 g, 1 mmol), and the mixture was refluxed for 2 h. The resulting red-colored solution was reduced to 10 mL. To this red-colored solution, under stirring, was dropwise added a methanol solution (5 mL) of nickel(II) perchlorate hexahydrate (0.366 g, 1 mmol). To the resulting green solution was dropwise added a methanol solution (2 mL) of triethylamine (0.101 g, 1 mmol). The color of the solution changed to red. After 1 h, an aqueous solution (5 mL) of NaN_3 (0.260 g, 4 mmol) was added dropwise to the stirred solution. After stirring for an additional 2 h, the green solution was filtered to remove any suspended particles and the green filtrate was allowed to evaporate at room temperature. After a few days, a green powdered compound was deposited, which was collected by filtration and washed with cold methanol. Recrystallization from ethanol produced a green crystalline compound containing diffraction quality crystals. The deposited crystalline compound was collected by filtration and washed with cold ethanol. Yield: 0.315 g (80%). Anal. Calcd for $C_{32}H_{50}N_{10}O_6Ni_2$: C, 48.76; H, 6.39; N, 17.77. Found: C, 48.89; H, 6.20;

Table 1. Crystallographic Data for 1 and 2

	1	2
empirical formula	$C_{32}H_{50}N_{10}O_6Ni_2$	$C_{32}H_{38}N_9O_{12}ClNi_2$
fw	788.24	893.58
cryst color	green	green
cryst syst	orthorhombic	monoclinic
space group	*Pbca*	$P2_1/c$
a [Å]	12.0237(4)	17.7887(11)
b [Å]	20.8688(6)	15.8087(10)
c [Å]	29.5810(9)	15.5453(10)
α [deg]	90.00	90.00
β [deg]	90.00	113.912(2)
θ [deg]	90.00	90.00
V [Å^3]	7422.5(4)	3996.4(4)
Z	8	4
temperature [K]	293(2)	296(2)
2θ [deg]	2.76−50.76	2.50−56.08
μ [mm^{-1}]	1.070	1.079
λ (Mo Kα) [Å]	0.71073	0.71073
ρ_{calcd} [g cm^{-3}]	1.411	1.485
$F(000)$	3328	1848
abs corr	multiscan	multiscan
index ranges	$-14 \le h \le 12$	$-22 \le h \le 22$
	$-25 \le k \le 25$	$-20 \le k \le 20$
	$-35 \le l \le 35$	$-20 \le l \le 20$
reflns collected	85 963	52 822
independent reflns (R_{int})	6815 (0.0939)	9431(0.0595)
R_1[a]/ wR_2[b] ($I > 2\sigma(I)$)	0.0333/0.0942	0.0456/0.1315
R_1[a]/wR_2[b] (for all data)	0.0555/0.1140	0.0910/0.1615

[a] $R_1 = [\Sigma||F_o| - |F_c||/\Sigma|F_o|]$. [b] $wR_2 = [\Sigma w(F_o^2 F_c^2)^2/\Sigma wF_o^4]^{1/2}$.

N, 17.86. Selected FT-IR data on KBr (cm^{-1}): ν(H_2O), 3350m; ν(azide), 2074vs, 2051vs; ν(C═N), 1635vs.

Data for **2**: Yield, 0.383 g (85%). Anal. Calcd for $C_{32}H_{46}N_9O_{12}ClNi_2$: C, 42.63; H, 5.14; N, 13.98. Found: C, 42.50; H, 5.20; N, 13.85. Selected FT-IR data on KBr (cm^{-1}): ν(H_2O), 3405m; ν(azide), 2069vs; ν(C═N), 1633vs.

Crystal Structure Determination of 1 and 2. Crystallographic data for **1** and **2** are summarized in Table 1. X-ray diffraction data were collected on a Bruker-APEX II SMART CCD diffractometer at 293 K for **1** and 296 K for **2** using graphite-monochromated Mo Kα radiation (λ = 0.71073 Å). For data processing and absorption correction the packages SAINT[26a] and SADABS[26b] were used. The structures were solved by direct and Fourier methods and refined by full-matrix least-squares based on F^2 using the SHELXTL[26c] and SHELXL-97 packages.[26d] All hydrogen atoms of **1** were located from difference Fourier maps.

During development of the structure of **2** it became apparent that few atoms were each disordered over two sites. These disordered atoms are C(10), C(11), C(12), and O(6) of one of the morpholine rings and O(10), O(11), and O(12) of the perchlorate anion. This was allowed for, and the final linked occupancy parameters for these disordered atoms are 0.60 and 0.40 for C(10), C(11), C(12), O(10), and O(11), 0.50 and 0.50 for O(6), and 0.70 and 0.30 for O(12). All hydrogen atoms except the coordinated solvent water hydrogen atoms were positioned geometrically (aromatic C−H 0.95 Å, ethyl C−H 0.99 Å, and methyl C−H 0.98 Å) and refined using a riding model with the isotropic displacement parameters fixed at U_{iso}(H) = 1.2 times U_{eq} of the parent carbon atom for the aromatic and ethyl hydrogen atoms and U_{iso}(H) = 1.5 times U_{eq} of the parent carbon atom for the methyl hydrogen atoms.

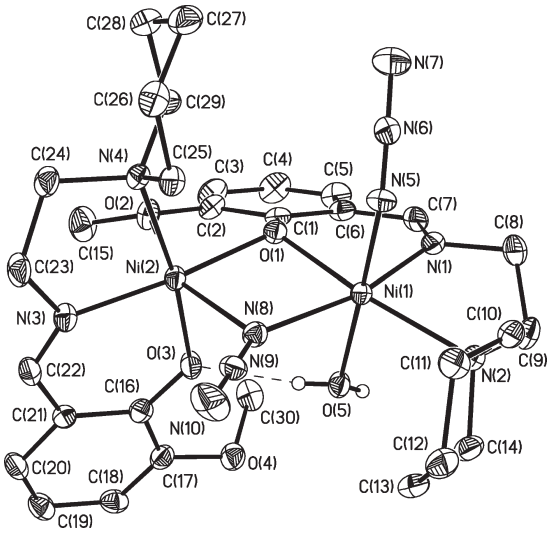

Figure 1. Crystal structure of $[Ni^{II}_2(L^1)_2(\mu_{1,1}\text{-}N_3)(N_3)(H_2O)]\cdot CH_3CH_2OH$ (**1**). Hydrogen atoms, except those of the water molecule, and solvated ethanol molecule are omitted for clarity.

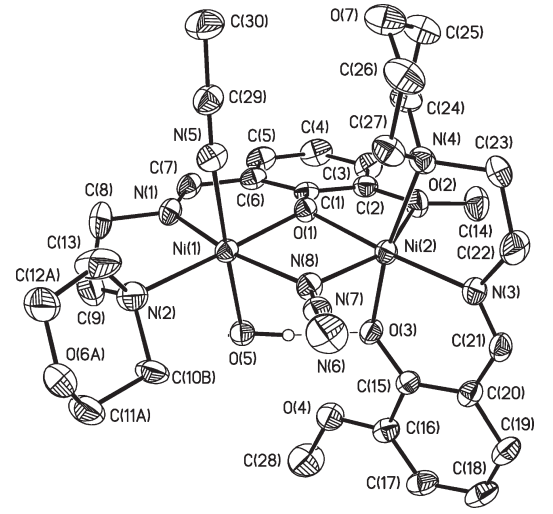

Figure 2. Crystal structure of $[Ni^{II}_2(L^2)_2(\mu_{1,1}\text{-}N_3)(CH_3CN)(H_2O)](ClO_4)\cdot H_2O\cdot CH_3CN$ (**2**). Hydrogen atoms, except those of the coordinated water molecule, solvated acetonitrile, and water molecules, and the perchlorate anion are omitted for clarity. Of the two sites of the disordered atoms, that with major occupancy is shown.

Using anisotropic treatment for the non-hydrogen atoms and isotropic treatment for the hydrogen atoms, the final refinements converged at the R_1 values ($I > 2\sigma(I)$) of 0.0333 and 0.0456 for **1** and **2**, respectively.

RESULTS AND DISCUSSION

Description of the Structures of 1 and 2. The crystal structures of $[Ni^{II}_2(L^1)_2(\mu_{1,1}\text{-}N_3)(N_3)(H_2O)]\cdot CH_3CH_2OH$ (**1**) and $[Ni^{II}_2(L^2)_2(\mu_{1,1}\text{-}N_3)(CH_3CN)(H_2O)](ClO_4)\cdot H_2O\cdot CH_3CN$ (**2**) are shown in Figures 1 and 2, respectively. The structures reveal that both are dinickel(II) compounds containing two deprotonated ligands, $[L^1]^-$ for **1** and $[L^2]^-$ for **2**. Except the occupation of a coordination position of a metal center, Ni(1), by a nitrogen atom N(5) of a monodentate azide anion in **1** and by the

dx.doi.org/10.1021/ic200833y |*Inorg. Chem.* 2011, 50, 7257–7267

Table 2. Selected Bond Lengths (Å) and Angles (deg) of 1 and 2

	1	2		1	2
Ni(1)−N(5)	2.093(2)	2.125(3)	Ni(2)−N(4)	2.178(2)	2.215(3)
Ni(1)−O(5)	2.084(2)	2.108(3)	Ni(2)−O(3)	2.004(2)	2.012(2)
Ni(1)−N(1)	2.013(2)	1.998(3)	Ni(2)−O(2)	2.281(2)	2.276(2)
Ni(1)−N(2)	2.224(2)	2.160(3)	Ni(2)−N(3)	2.000(2)	1.986(3)
Ni(1)−N(8)	2.138(2)	2.125(3)	Ni(2)−N(8)	2.083(2)	2.115(3)
Ni(1)−O(1)	2.0583(19)	2.017(2)	Ni(2)−O(1)	2.0120(19)	1.994(2)
N(5)−Ni(1)−O(5)	174.63(9)	176.10(12)	N(4)−Ni(2)−O(3)	171.77(8)	170.29(10)
N(1)−Ni(1)−N(8)	164.36(9)	167.26(11)	N(8)−Ni(2)−O(2)	153.34(8)	152.55(9)
N(2)−Ni(1)−O(1)	168.89(8)	173.64(12)	N(3)−Ni(2)−O(1)	172.50(9)	175.04(10)
N(1)−Ni(1)−O(1)	86.73(8)	89.41(10)	O(2)−Ni(2)−O(1)	74.36(7)	74.17(8)
N(1)−Ni(1)−N(2)	82.63(9)	84.86(13)	O(2)−Ni(2)−N(3)	98.23(9)	101.08(11)
N(1)−Ni(1)−O(5)	93.40(9)	90.24(12)	O(2)−Ni(2)−O(3)	84.04(8)	86.30(9)
N(1)−Ni(1)−N(5)	91.65(9)	87.52(11)	O(2)−Ni(2)−N(4)	92.51(8)	89.26(10)
O(1)−Ni(1)−N(8)	77.75(8)	77.93(9)	O(1)−Ni(2)−N(8)	80.06(8)	78.67(9)
O(1)−Ni(1)−O(5)	89.64(8)	87.59(10)	O(1)−Ni(2)−O(3)	90.00(8)	91.27(9)
O(1)−Ni(1)−N(5)	92.51(9)	89.19(11)	O(1)−Ni(2)−N(4)	96.28(8)	95.83(10)
N(2)−Ni(1)−O(5)	87.83(9)	89.67(11)	N(3)−Ni(2)−O(3)	90.35(9)	89.83(11)
N(2)−Ni(1)−N(5)	90.97(9)	93.30(12)	N(3)−Ni(2)−N(4)	82.73(9)	82.54(11)
N(2)−Ni(1)−N(8)	112.75(9)	107.71(12)	N(3)−Ni(2)−N(8)	107.44(10)	106.16(11)
O(5)−Ni(1)−N(8)	84.68(9)	87.79(11)	O(3)−Ni(2)−N(8)	88.63(9)	90.43(10)
N(5)−Ni(1)−N(8)	90.96(9)	93.70(11)	N(4)−Ni(2)−N(8)	97.67(9)	97.45(11)
Ni(1)−N(8)−Ni(2)	98.02(10)	97.02(11)	Ni(1)−O(1)−Ni(2)	103.02(8)	104.68(9)

nitrogen atom N(5) of an acetonitrile molecule in **2**, the ligand environment in both compounds is similar. Of the two phenoxo oxygen atoms of two $[L^1]^-/[L^2]^-$, one oxygen atom O(1) bridges the two metal centers (Ni(1) and Ni(2)) while the second oxygen O(3) acts as a monodentate ligand and is coordinated to the Ni(2) center. Again, of the two methoxy oxygen atoms of two $[L^1]^-/[L^2]^-$, O(2) is coordinated to Ni(2) while the second oxygen atom O(4) is noncoordinated. The piperidine (for **1**)/morpholine (for **2**) nitrogen atoms ((N(2), N(4)) and imine nitrogen atoms (N(1), N(3)) of each of the two $[L^1]^-/[L^2]^-$ are coordinated to each of the two metal centers. In addition to the phenoxo bridge, the metal centers in the dinuclear core are also bridged by the nitrogen atom N(8) of an end-on azide ligand. The remaining coordination position of Ni(1) is satisfied by the oxygen atom of a water molecule. Thus, both metal centers are hexacoordinated, but the coordination environment of Ni(1) and Ni(2) consists of a different set of donor atoms. The μ-phenoxo-$\mu_{1,1}$-azide dinickel(II) core in **1** is electroneutral. In contrast, the μ-phenoxo-$\mu_{1,1}$-azide dinickel(II) core in **2** is monopositively charged, which is balanced by a perchlorate counteranion. One ethanol molecule in **1** and one water and one acetonitrile molecule in **2** are present as solvent(s) of crystallization.

The bond lengths and angles in the coordination environment of the metal centers in **1** and **2** are listed in Table 2. The Ni(2) centers in **1** and **2** are similarly coordinated and follow a similar trend in their bond distances; the bond distances involving the bridging and monodentate phenoxo oxygen atoms and the imine nitrogen atom, ca. 2 Å, are shorter than other three bond lengths, which follow the order Ni−O(methoxy) > Ni−N(piperidine/morpholine) > Ni−N($\mu_{1,1}$-N_3). In contrast to the Ni(2) center, the trend of bond distances is slightly different than the Ni(1) centers in **1** and **2** because these are not similarly coordinated. For the Ni(1) center in **2**, the bond distances involving the bridging phenoxo oxygen atom and the imine nitrogen atom, ca. 2 Å, are shorter than other four bond lengths, which follow the order Ni−N(morpholine) > Ni−N($\mu_{1,1}$-N_3) ≈ Ni−N(acetonitrile) > Ni−O(water). For the Ni(1) center in **1**, the order of bond lengths is Ni−N(piperidine) > Ni−N($\mu_{1,1}$-N_3) > Ni−N(N_3) ≈ Ni−O(water) > Ni−O(bridging phenoxo) > Ni−N(imine). The ranges of bond lengths are significantly wide; from ca. 2 to 2.224(2), 2.160(3), 2.281(2), and 2.276(2) Å for Ni(1) in **1**, Ni(1) in **2**, Ni(2) in **1**, and Ni(2) in **2**, respectively, in which the bond lengths involving ethereal oxygen or piperidine/morpholine nitrogen atoms are the longest.

The hexacoordinated environment of both metal centers is distorted octahedral. For Ni(1), the basal plane is defined by the bridging phenoxo oxygen atom, O(1), and the imine, piperidine (for **1**)/morpholine (for **2**), and bridging azide nitrogen atoms, N(1), N(2), and N(8), respectively, while the terminal azide (for **1**)/acetonitrile (for **2**) nitrogen atom, N(5), and the water oxygen atom, O(5), occupy the axial positions. In the case of Ni(2), the bridging phenoxo and ethereal oxygen atoms, O(1) and O(2), respectively, and the bridging azide and imine nitrogen atoms, N(8) and N(3), respectively, define the basal plane, while the piperidine (for **1**)/morpholine (for **2**) nitrogen atom, N(4), and the monodentate phenoxo oxygen atom, O(3), are present in the axial positions. The ranges of the transoid angles are 164.36(9)−174.63(9)° for Ni(1) in **1**, 167.26(11)−176.10(12)° for Ni(1) in **2**, 153.34(8)−172.5(9)° for Ni(2) in **1**, and 152.55(9)−175.04(10)° for Ni(2) in **2**. The ranges of the cisoid angles are 77.75(8)−112.75(9)° for Ni(1) in **1**, 77.93(9)−107.71(12)° Ni(1) in **2**, 74.36(7)−107.44(10)° for Ni(2) in **1**, and 74.17(8)−106.16(11)° for Ni(2) in **2**. Clearly, both the transoid and the cisoid angles deviate significantly from ideal values of an octahedral geometry. On the other hand, in both **1** and **2** the displacement of the metal centers and average

dx.doi.org/10.1021/ic200833y |*Inorg. Chem.* 2011, 50, 7257–7267

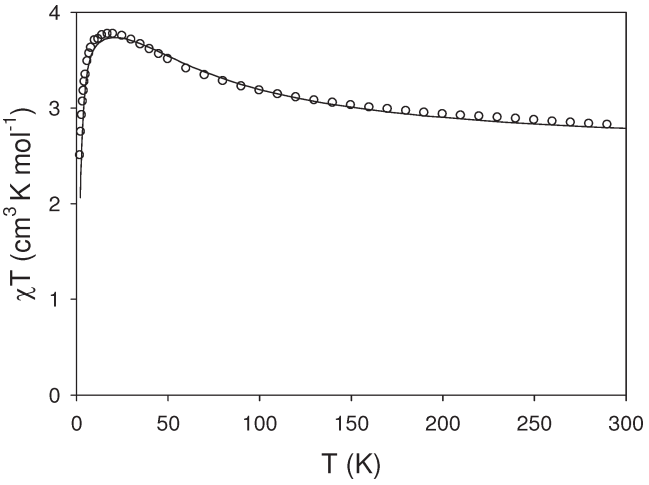

Figure 3. χT versus T plot for **1**. The solid line is the calculated susceptibility using MAGPACK; see text for more information.

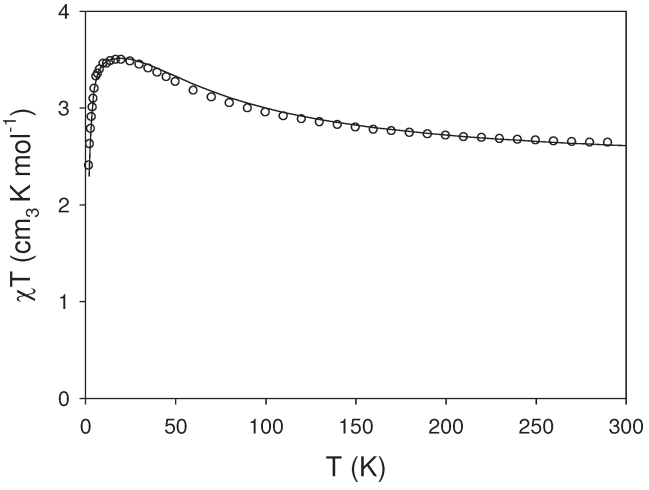

Figure 4. χT versus T plot for **2**. The solid line is the calculated susceptibility using MAGPACK; see text for more information.

deviation of the constituent atoms from the corresponding least-squares basal planes are small, less than 0.1 Å, which may apparently indicate slight distortion of the coordination environment.

The Ni(1)−O(1)−Ni(2) bridge angle (103.02(8)° in **1**; 104.68(9)° in **2**), Ni(1)−N(8)−Ni(2) bridge angle (98.02(10)° in **1**; 97.02(11)° in **2**), and metal···metal separation (3.186 Å in **1**; 3.176 Å in **2**) in the dinuclear core are not very different in the two complexes. The dihedral angle between the basal planes, N(1)N(2)N(8)O(1) and N(3)N(8)O(1)O(2), of the two coordination environments is also almost the same for the two complexes, 14.7° in **1** and 14.8° in **2**. These dihedral angles and also the dihedral angle (12.7° in **1** and 15.4° in **2**) between the two bridges, Ni(1)O(1)Ni(2) and Ni(1)N(8)Ni(2), indicate that the bridging moiety is slightly twisted.

As shown in Figures 1 and 2, there exists a strong intramolecular hydrogen-bonding interaction in both compounds involving one hydrogen atom (H(5WA)) of the coordinated water molecule ($H_2O(5)$) and the monodentate phenoxo oxygen atom (O(3)). This provides an additional bridging moiety, Ni(2)−O(3)···H(5WA)−O(5)−Ni(1). The O(3)···O(5) distances are 2.655 Å in **1** and 2.658 Å in **2**, while the O(5)−H(5WA)···O(3) angles

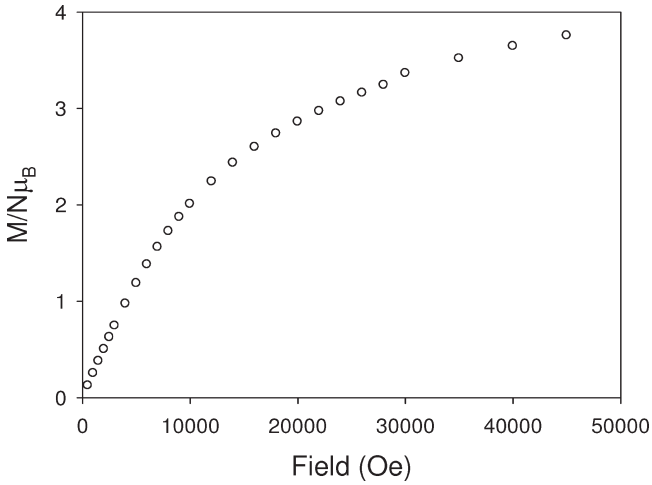

Figure 5. Magnetization versus field plot for **1** at 2 K.

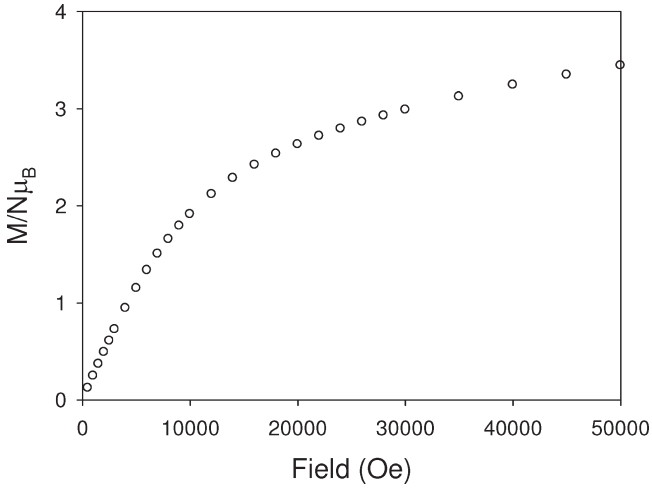

Figure 6. Magnetization versus field plot for **2** at 2 K.

are 163.5° and 166.9° in **1** and **2**, respectively, indicating that the hydrogen bond is strong.

Magnetic Properties. DC magnetic susceptibility data were collected for crushed crystalline samples of **1** and **2** at an applied magnetic field of 0.7 T in the 2−300 K temperature range. The data are shown in Figures 3 and 4 as χT versus T plots. The profiles are similar for the two complexes. The χT value, 2.8 cm^3 K mol^{-1} for **1** and 2.6 cm^3 K mol^{-1} for **2**, at 300 K is above the expected value of 2.4 cm^3 K mol^{-1} for two nickel(II) ions with $g = 2.2$ and $S = 1$. As temperature decreases, the χT product increases until a maximum is reached at 20 K. This indicates ferromagnetic coupling between the nickel(II) centers in both complexes. This is confirmed by the magnetization versus field behavior at 2 K, shown in Figure 5 for **1** and Figure 6 for **2**. The observed magnetization tends to saturation at a value of 4 μ_B, indicating an $S = 2$ ground state achieved due to ferromagnetic coupling between the nickel(II) ions.[27] Below 20 K a decrease in the χT product is observed, and this might be associated with the ground state zero-field splitting and/or intermolecular interactions.

In order to properly model the experimental magnetic data of a nickel(II) dinuclear complex such as **1** and **2**, the anisotropy of

dx.doi.org/10.1021/ic200833y |*Inorg. Chem.* 2011, 50, 7257–7267

Table 3. Magnetic and Structural Parameters of the Five μ-Phenoxo-$\mu_{1,1}$-Azide Nickel(II) Compounds

compound no.	J_{exp} (cm^{-1})	J_{DFT} (cm^{-1})	Ni−O−Ni (deg)	Ni−N−Ni (deg)	Ni−O (Å)	average Ni−O (Å)	asymmetry in Ni−O (Å)	Ni−N (Å)	average Ni−N (Å)	asymmetry in Ni−N (Å)	ref
1	16.6	15.8	103.0	98.0	2.01, 2.06	2.035	0.05	2.08, 2.14	2.11	0.06	this work
2	16.9	15.35	104.7	97.0	1.99, 2.02	2.005	0.03	2.12, 2.11	2.115	0.01	this work
3	5.0	14.1[a]	106.9	96.3	1.99, 1.99	1.99	0.00	2.09, 2.21	2.15	0.12	2d
4	25.6	18.5[a]	106.7	96.5	1.98, 1.99	1.985	0.01	2.13, 2.15	2.14	0.02	10a
5	2.85	12.65/10.05	102.3	95.6	2.00, 2.04	2.02	0.04	2.11, 2.14	2.125	0.03	10b

[a] Density functional J values have been computed in this work.

the hexacoordinated nickel(II) ions must be taken into account. This was done using the full-matrix diagonalization software MAGPACK,[28] which allows a calculation of the susceptibility and magnetization data using a model that includes the zero-field splitting parameter D of each single ion. The exchange Hamiltonian used was $\hat{H} = -2J[\hat{S}_1\hat{S}_2] + \Sigma D_{Ni}\hat{S}_{iz}^2$. The best simulations of the experimental data are shown in Figures 3 and 4 as solid lines; the fitting parameters were $J = 16.6\ cm^{-1}$, $g = 2.25$, and $D(Ni1) = D(Ni2) = -7.3\ cm^{-1}$ for **1** and $J = 16.92\ cm^{-1}$, $g = 2.2$, and $D(Ni1) = D(Ni2) = -6.41\ cm^{-1}$ for **2**. The D value for the two nickel(II) ions is in agreement with the expected single-ion values reported in the literature.[15b,d]

Discussion on Magnetic Behavior of 1, 2, and Related Compounds in Terms of Structural Parameters. Previously, single-crystal X-ray structures and magnetic properties of three μ-phenoxo-$\mu_{1,1}$-azide dinickel(II) compounds have been reported.[2d,10] The magnetic and structural parameters of **1**, **2**, and three previously published compounds (**3**, **4**, and **5**) are compared in Table 3. All five compounds are ferromagnetically coupled with J values ranging between 2.85 and 25.6 cm^{-1}. The pair of compounds **3** and **4** in Table 3 is unique because, except the individual Ni−N distances and therefore asymmetry in Ni−N distances, all other structural parameters including even the average Ni−N distance are almost identical. They exhibit a significantly different ferromagnetic interaction, 5.0 cm^{-1} for **3** and 25.6 cm^{-1} for **4**, which clearly indicates the role of individual Ni−N bond distances and asymmetry (0.12 Å in **3** and 0.02 Å in **4**) in bond distances on the extent of interaction. As rationalized from DFT calculations (see below), compounds **3** and **4** therefore present experimental evidence of the role of asymmetry in bond distances on exchange interaction in heterobridged compounds; keeping all other factors the same, the ferromagnetic interaction increases if asymmetry decreases on these two complexes. However, as it is absolutely accidental to get compounds having most of the structural parameters identical, it is difficult to rationalize the relative magnitudes of J values in most cases. For example, compounds **2** (asymmetry = 0.01 Å) and **5** (asymmetry = 0.03 Å) should exhibit a strong interaction as in compound **4** (asymmetry 0.02 Å) on the basis of the asymmetry factor, but the J values are significantly different (25.6 cm^{-1} in **4**, 16.92 cm^{-1} in **2**, and only 2.85 cm^{-1} in **5**). Again, in comparison to **4** ($J = 25.6\ cm^{-1}$), compounds **1** ($J = 16.6\ cm^{-1}$) and **2** ($J = 16.92\ cm^{-1}$) should be more ferromagnetic on the basis of Ni−O−Ni and Ni−N−Ni angles and average Ni−O distance but less ferromagnetic on the basis of the average Ni−N distance, the later is actually the observed result. More comparisons on the structural and magnetic parameters of the compounds in Table 3 can result in the same conclusion that the ferromagnetic interaction and the relative extent of ferromagnetic interaction arise due to composite effects of several structural parameters. A comparison along structures **1**−**5** reveals that, despite the fact that Ni−N asymmetry plays a proactive role in determining the strength of J values, other structural parameters should also been taken into consideration to explain the trend observed for complexes **1**−**5**. To probe this further, DFT calculations have been used to develop several magneto-structural correlations in the following section.

Theoretical Studies. DFT-computed magnetic exchange interactions for complexes **1**−**4** in this work and **5**[10b] are given in Table 3. For complexes **1** and **2**, an excellent agreement to the experimental J value has been obtained. For complexes **3** and **4**, although the computed magnetic exchange interactions are not that accurate compared to experimental values, the trend of a large ferromagnetic interaction for a less asymmetric Ni−N bond length is reproduced. We will begin our discussion with complexes **1** and **2**. The magnetic exchange interactions in complexes **1** and **2** are mediated by (i) one $\mu_{1,1}$-azido group, (ii) one μ-phenoxo group, and (iii) a hydrogen-bonding interaction via the exchange pathway Ni(2)−O(3)···H(5WA)−O(5)−Ni(1). Among these three pathways, (i) and (ii) are expected to play an important role in mediating the coupling between the metal centers.

To understand the role of dissimilar bridges on magnetic coupling and its complementarity and counter-complementarity effects, computations have been performed on model complexes of **1**. Here, a breakdown approach has been adopted where the magnetic exchange pathways through the $\mu_{1,1}$-azido and μ-phenoxo groups were successively removed to produce different model complexes and a J value has been computed on these model complexes. The first model, removing the $\mu_{1,1}$-azido group from **1** ($[Ni^{II}_2(L^1)_2(N_3)(H_2O)]^+$; **1a**), yields a J value of $-23.3\ cm^{-1}$, while removing only the μ-phenoxo bridge ($[Ni^{II}_2(\mu_{1,1}\text{-}N_3)(L^1)(L^{1a})(N_3)(H_2O)]^+$; L^{1a} = the bridging oxygen atom of the μ-phenoxo group substituted by hydrogen atom on the L^1 ligand, see Figure S1 in the Supporting Information; **1b**) from **1** yields a J of $-1.1\ cm^{-1}$. Removing both bridges ($[Ni^{II}_2(L^{1a})_2(N_3)(H_2O)]^{2+}$; **1c**) from **1** leads to a J value of $-17.7\ cm^{-1}$. To avoid the differences in coordination number between **1** and the model complexes, point charges have been placed at the coordination position with the Mulliken charges computed for the respective atom on **1**. Surprisingly, all computed exchange interactions are antiferromagnetic in nature compared to that of complex **1**. Model **1c** where both $\mu_{1,1}$-azido and μ-phenoxo are absent has strong antiferromagnetic interactions. Since the bridges have been removed, the antiferromagnetic interactions are likely to be due to the direct interaction of the magnetic orbitals and the hydrogen-bonded exchange interaction pathway discussed earlier. If we add a $\mu_{1,1}$-azido bridge to this model (**1a**), the interaction only due to the azido group can

dx.doi.org/10.1021/ic200833y |Inorg. Chem. 2011, 50, 7257–7267

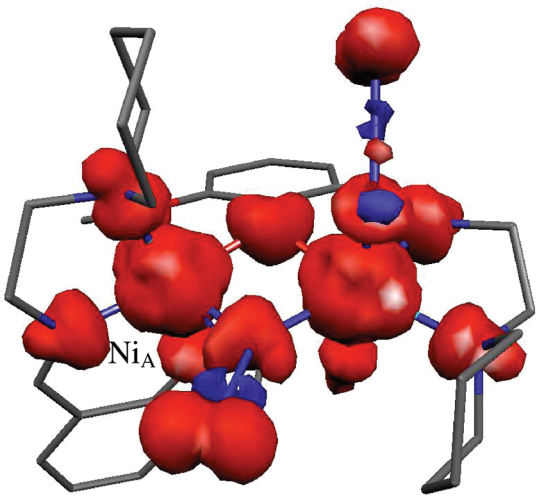

Figure 7. DFT-computed spin density plot for the high-spin state of complex **1**: red, positive spin density; blue, negative spin density.

be evaluated. The increase in the antiferromagnetic interaction upon addition of an azido group reveals that this group exhibits a complementarity effect. If the μ-phenoxo group is added to model **1c**, the interaction becomes weakly antiferromagnetic; this reveals that the phenoxo group exhibits a counter-complementarity effect. However, the combined effect of two bridges leads to a net ferromagnetic interaction and reveals that a complex ferro−antiferromagnetic pathway is at play in complex **1**. As shown in the orbital model (see below) the frontier p-type orbitals of the azide are interacting with the antisymmetric orbitals of the Ni atom, leading to an enhancement in the gap between the magnetic orbitals, which is directly proportional to the antiferromagnetic exchange interactions.

The computed spin density plot for the high-spin state of complex **1** is shown in Figure 7. The shapes of the spin density on the Ni atoms are octahedral. The two Ni atoms have a spin density of 1.66 (Ni$_A$; see Figure 7) and 1.68, which reveals that the two Ni atoms are not equivalent by symmetry. Both the bridging phenoxo oxygen (0.08) and the azide nitrogen (0.04) atoms have large positive spin density, ruling out the presence of a spin polarization mechanism for the magnetic coupling. The azido nitrogen atom has a relatively smaller spin density compared to the phenoxo oxygen atom, and this is probably due to the shorter Ni−O bond lengths compared to Ni−N distances and also to the polarization within the N_3 unit (note a negative spin density at the middle N of the bridging azido group). The similar computed spin density plots for the high-spin state of complexes **2**, **3**, and **4** are shown, Figures S2−S4 and discussed in the Supporting Information.

Orbital Analysis on the Role of Asymmetry. The suitability of DFT orbitals for qualitative analysis has been found to be valid on many occasions and provided many useful insights.[17a,21] Although the net exchange is ferromagnetic, the net exchange interaction results due to the counterplay of ferro−antiferromagnetic contributions. According the Kahn−Briat model,[29] J has been related to the overlap between nonorthogonal localized magnetic orbitals. On many occasions empty magnetic orbitals are shown to be superior to represent the Kahn−Briat model and were successfully employed for qualitative interpretation.[17b] Therefore, we decided to use these orbitals for our orbital analysis. For interaction between two Ni^{II} ions the following four overlap integrals should be considered: (i) Ni_A-d_{z^2}|p|Ni_B-d_{z^2}, (ii) Ni_A-d_{z^2}|p|Ni_B-$d_{x^2-y^2}$, (iii) Ni_A-$d_{x^2-y^2}$|p|Ni_B-$d_{x^2-y^2}$, and (iv) Ni_A-$d_{x^2-y^2}$|p|Ni_B-d_{z^2}. Overlaps (ii) and (iv) are expected to be different as the two Ni atoms are asymmetric in nature.

MO analysis has been performed on complexes **1**, **3**, and **4** to understand the cause of asymmetry on the electronic structure and hence the magnetic coupling. Qualitative magnetic orbitals are drawn based on the high spin, and broken symmetry SOMOs of complexes **1**, **3**, and **4** together with the overlap integral computed between their BS magnetic orbitals (see Figure S5 in the Supporting Information for the DFT-computed BS orbitals) are shown in Scheme 2. There is tremendous change in the orientation of the magnetic orbitals across this series. Here, we begin our discussion with complex **3** where a least ferromagnetic J has been encountered (see Table 3). For complex **3** the d_{z^2} orbitals have head-to-head overlap, and a significant $d_{x^2-y^2}$−$d_{x^2-y^2}$ interaction is also encountered. From the overlap integral values, it is apparent that the strongest interaction is for the d_{z^2}−d_{z^2} pair but all four interactions are significant in this case. For complex **1** where J is intermediate between **3** and **4**, a different orientation is encountered. Here, the orientation of the $d_{x^2-y^2}$ and d_{z^2} orbitals is perpendicular to one another. This perpendicular orientation of the orbitals is likely to cause less overlap between the magnetic orbitals, and hence, a relatively stronger ferromagnetic interaction is expected. From the overlap integral values this is apparent, i.e., complex **1** has in general smaller overlap integral values with the strongest interaction observed for the $d_{x^2-y^2}$−$d_{x^2-y^2}$ pair while one of the $d_{x^2-y^2}$−d_{z^2} pairs has negligible interaction. This leads to a decrease in the antiferromagnetic contribution, and thus, the net exchange is expected to be more ferromagnetic than complex **3**. For complex **4** where the largest positive J is encountered, again a different orientation is detected where the d_{z^2} and $d_{x^2-y^2}$ orbitals are parallel to each other, leading to a smaller overlap integral than complex **1** and a larger ferromagnetic J as observed by the experiments. This difference in orientation is likely to be caused due to the asymmetry of the Ni−N bond lengths as this is the significant structural difference perceived across the series.

Magneto-Structural Correlations of μ-Phenoxo-$\mu_{1,1}$-Azide Dinickel(II) Systems. Since the complexes possess dissimilar bridges there are many parameters which can affect the magnitude of J. Here, the exchange interaction propagated mainly through the phenoxo and end-on azido bridges and the structural parameters relevant to this two bridges should be considered to understand the magnetic behavior of a compound having a μ-phenoxo-$\mu_{1,1}$-azide bridging moiety. Therefore, the metal−phenoxo−metal bridge angle and metal−phenoxo bond distance should have roles to govern the exchange interaction propagated through the phenoxo bridge, while the metal−azide−metal bridge angle and metal−azide bond distance are the key parameters to result in the nature and magnitude of interaction propagated through the azide bridge. Although some experimental and theoretical structure−property relationships have been determined for bis(μ-phenoxo) dinickel(II)[2b] and also in bis($\mu_{1,1}$-azide) dinickel(II)[4a] compounds, magneto-structural correlations for μ-phenoxo-$\mu_{1,1}$-azide dinickel(II) compounds are relevant to establish a better understanding of their magnetic properties. Therefore, as described below, we established density functional theoretical correlations for μ-phenoxo-$\mu_{1,1}$-azide dinickel(II) compounds.

We developed three different correlations on compound **1**. The presence of dissimilar bridges prevents variation of only one structural parameter at a time to develop correlations; therefore,

Scheme 2. Qualitative SOMOs Involved in the Exchange Coupling of 1, 3, and 4 Together with the Overlap Integral Computed for Their Corresponding Broken-Symmetry Counterpart

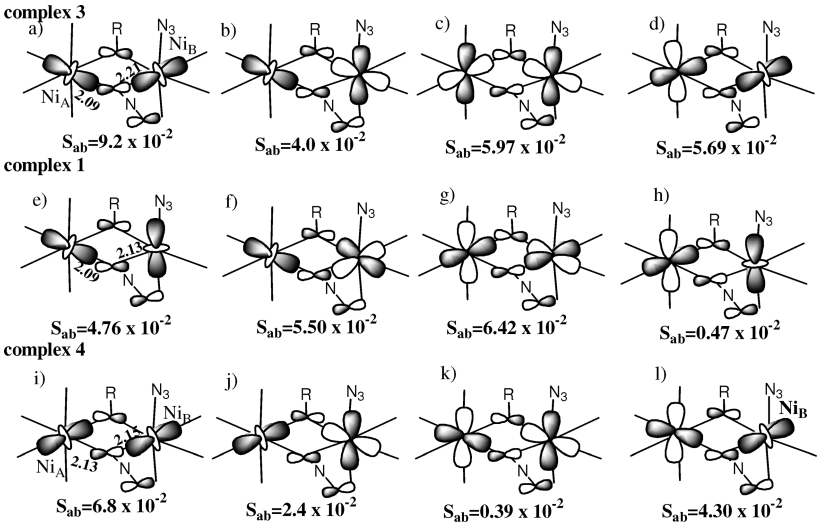

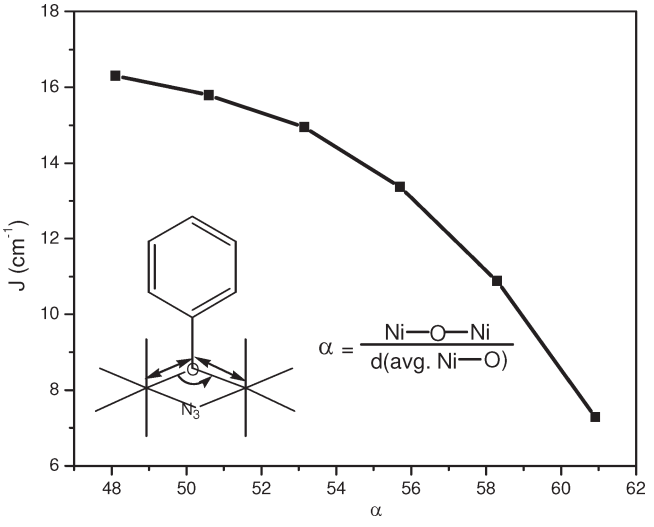

Figure 8. Magneto-structural correlations developed by varying α versus *J*.

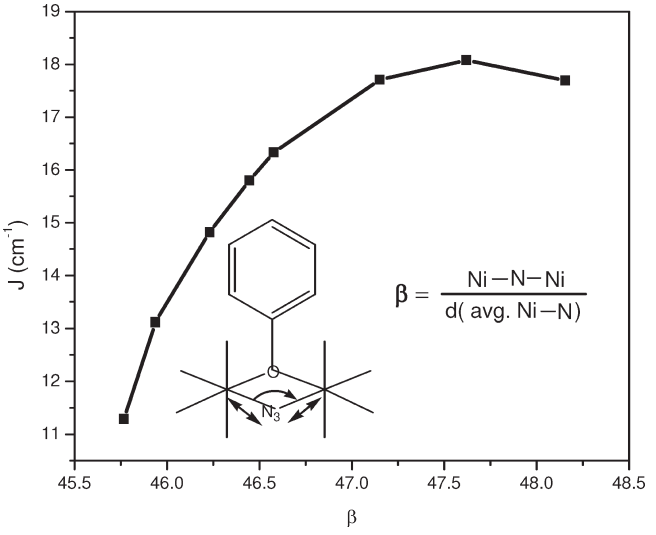

Figure 9. Magneto-structural correlations developed by varying β versus *J*.

in all correlations two parameters, angles as well as the Ni—O or Ni—N distances, were varied. The first correlation is developed by varying the Ni—O—Ni angle as well as the average Ni—O distance. To underpin the role of asymmetry on the bond lengths, the asymmetry present in the bond distances was maintained throughout. A new parameter α is defined (see below) to take into account the variation of the two parameters, and the correlation of *J* versus α is shown in Figure 8.

$$\alpha = \frac{\text{Ni—O—Ni}}{d(\text{avg.Ni—O})}$$

This correlation indicates that the ferromagnetic interaction decreases with an increase in the α parameter. Eventually this means that the large Ni—O—Ni angle or short Ni—O distance tends to decrease the magnitude of ferromagnetic *J* observed, and this is consistent with Ni—O—Ni angle correlations developed for different dinuclear and polynuclear structures[3b,c] (note, a double-*y*-plot where the two parameters were independently taken and plotted against *J* is given in Figure S6 in the Supporting Information). A larger Ni—O—Ni angle or shorter Ni—O distance is expected to increase the overlap integral between the magnetic orbitals shown in Scheme 2, and hence, the antiferromagnetic part of the exchange will increase, leading to a decrease in the net ferromagnetic *J*.

A second correlation is developed by varying the Ni—N—Ni bond angles as well the Ni—N distance simultaneously. Here, the Ni—N bond length asymmetry is maintained as in complex **1** (0.06 Å). The following parameter (β) is defined to describe this correlation

$$\beta = \frac{\text{Ni—N—Ni}}{d(\text{avg.Ni—N})}$$

This graph (Figure 9) reveals that the increase in β leads to an increase in the ferromagnetic *J*; however, there is a maximum

dx.doi.org/10.1021/ic200833y |*Inorg. Chem.* 2011, 50, 7257–7267

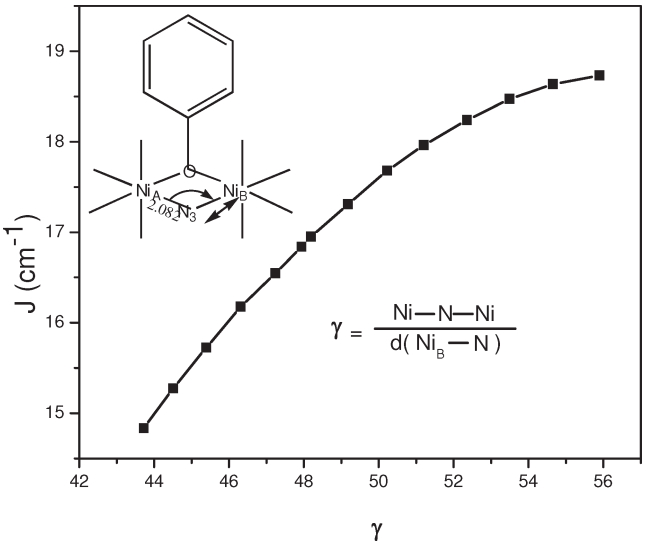

Figure 10. Magneto-structural correlations developed by varying γ versus J.

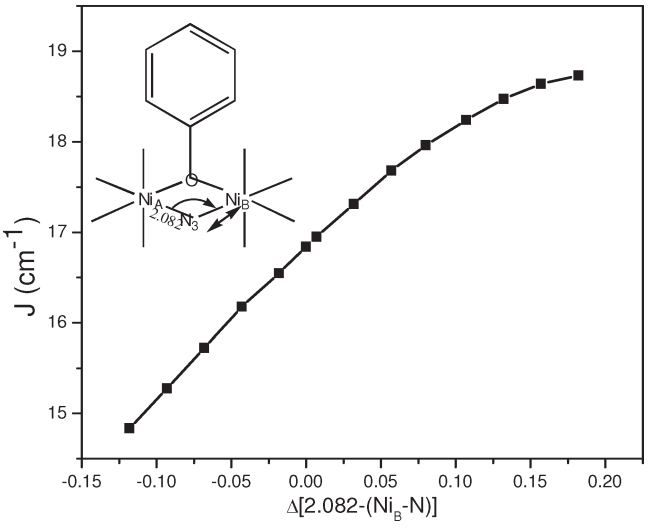

Figure 11. Asymmetry in the Ni—N distances versus J (note in this plot the variation in the Ni—N—Ni angle is ignored.).

observed at 106° after which the ferromagnetic interaction in fact decreases (see a double-y-plot where the two parameters were independently taken and plotted against J as given in Figure S7 in the Supporting Information). An increase in the Ni—N—Ni angle with an increase in the ferromagnetic interaction has been encountered in many binuclear Ni end-on azido complexes.[4a] Unlike the μ-phenoxo group which exhibits a counter-complementarity effect, the azido bridge exhibits a complementarity effect; thus, an increase of the angle leads to a larger ferromagnetic exchange.[2e,4a]

A third correlation has been developed to understand the role of Ni—N bond length asymmetry on the magnetic coupling. For this set of calculations, the phenoxo bridging moiety and one Ni—N bond length are kept constant (at 2.082 Å) while the second Ni—N bond length is varied, resulting in a variation of the Ni—N—Ni angle as well. A new parameter γ has been defined as follows

$$\gamma = \frac{\text{Ni—N—Ni}}{d(\text{Ni}_\text{B}\text{—N})}$$

The computed correlation is shown in Figure 10. This plot reveals that larger γ tends to increase the ferromagnetic J; however, saturation is reached at very large γ values. To understand how J correlates with the asymmetry (Δ), the change in the Ni—N—Ni angle is ignored and the asymmetry vs J is plotted in Figure 11. The shape of the curve resembles that of the J vs γ plot. In this graph the asymmetry is denoted in positive as well as negative values with reference to the fixed Ni_A—N distance of 2.082 Å. A negative value indicates that $d_{\text{NiB—N}} > 2.082$ Å, while a positive value indicates that $d_{\text{NiB—N}} < 2.082$ Å. Although the shape of the curve reveals a near-linearity relationship, the role of asymmetry differs. An increase in the negative asymmetry decreases the ferromagnetic interaction, while an increase in the positive asymmetry increases the ferromagnetic interaction, albeit this saturates at a larger value. It is clear from this plot that if the Ni_B—N distance is larger than 2.082 Å, an increase in asymmetry will lead to a smaller ferromagnetic J as in the case of complex **3** (the parameter Δ is −0.13 Å here). Less asymmetry will lead to an increase in J as

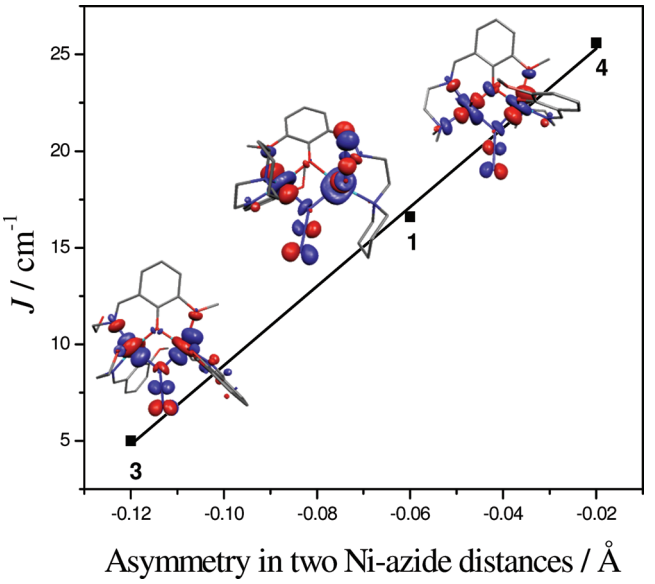

Figure 12. Linear magneto-structural correlation between exchange integral (J) and asymmetry in Ni—azide bond distances. Squares and lines indicate observed data and linear fit, respectively. The inset orbital diagram corresponds to the d_{z^2}—d_{z^2} empty-broken symmetry orbitals of complexes **3**, **1**, and **4** exhibiting the difference in the orientation.

in complex **1** (Δ = −0.06 Å here), and a further decrease will increase J further. Orbitals e) and f) given in Scheme 2 are expected to govern the role of Ni—N asymmetry on the magnetic coupling. As discussed before, elongation of Ni_B—N leads to a change in the orientation with a head-to-head overlap expected to occur at larger negative asymmetry. Although our experimental and theoretical studies explicitly reveal the nature of Ni—N asymmetry on the magnetic exchange, there are other structural parameters which were also varied simultaneously in our calculations. Therefore, other structural parameters such as bond angles, bond lengths, and dihedral angles also need to be considered to account for the variation of the exchange interaction in this type of complex.

dx.doi.org/10.1021/ic200833y |*Inorg. Chem.* 2011, 50, 7257–7267

CONCLUSIONS

As there are very few heterobridged discrete compounds of nickel(II), the compounds $[Ni^{II}_2(L^1)_2(\mu_{1,1}\text{-}N_3)(N_3)(H_2O)]\cdot CH_3CH_2OH$ (**1**) and $[Ni^{II}_2(L^2)_2(\mu_{1,1}\text{-}N_3)(CH_3CN)(H_2O)](ClO_4)\cdot H_2O\cdot CH_3CN$ (**2**) are important additions in the family of such systems. Observation of an ferromagnetic interaction in both **1** and **2** indicates that the ligand design has been successful in achieving ferromagneticaly coupled heterobridged complexes. Interestingly, the observed *J* values for both compounds **1** and **2** are well matched with *J* values obtained from broken symmetry density functional calculations. The magnetic exchange interactions of complex **1** together with the previously reported two complexes (**3** and **4**) reveal a linear correlation against asymmetry of the Ni−N distance as shown in Figure 12. The density functional calculations performed on the full structure of all complexes reveal an interesting analogy across this pattern where the orientation of the d_{z^2} orbitals seems to differ with respect to the asymmetry in the Ni−N distance. A large asymmetric structure enhances a head-to-head overlap, and hence, a large antiferromagnetic contributions is witnessed (see Figure 12). Several magneto-structural correlations have been developed, which reveals that the asymmetry plays a proactive role in the magnetic coupling. Designed syntheses of systems exhibiting ferromagnetic interaction, only the fourth and fifth examples of heterobridged μ-phenoxo-$\mu_{1,1}$-azido dinickel(II) compounds, close matching of experimental and theoretical *J* values, and, most importantly, determination of density functional theoretical magneto-structural correlations for not only μ-phenoxo-$\mu_{1,1}$-azido dinickel(II) compounds but also for any type of heterobridged systems are the major outcomes of the present investigation.

ASSOCIATED CONTENT

Supporting Information. Crystallographic data of **1** and **2** in CIF format; discussion on the spin density of **2**, **3**, and **4**; Figures S1−S7. This material is available free of charge via the Internet at http://pubs.acs.org.

AUTHOR INFORMATION

Corresponding Author

*E-mail: sm_cu_chem@yahoo.co.in (S.M.); rajaraman@chem.iitb.ac.in (G.R.); carolina.sanudo@qi.ub.es (E.C.S.).

ACKNOWLEDGMENT

Financial support from the Government of India through the Department of Science and Technology (SR/S1/IC-12/2008), University Grants Commission (Fellowship to S.S.), and Council for Scientific and Industrial Research (Fellowship to S.H.) is gratefully acknowledged. Crystallography was performed at the DST-FIST, India-funded Single Crystal Diffractometer Facility at the Department of Chemistry, University of Calcutta. E.C.S. acknowledges financial support from the Spanish Government (Grant CTQ2009/006959BQU and Ramón y Cajal contract). Financial support from the Government of India through the Department of Science and Technology (SR/S1/IC-41/2010) and generous seed money and computational resources to Indian Institute of Technology-Bombay is gratefully acknowledged.

REFERENCES

(1) (a) Kahn, O. *Molecular Magnetism*; VCH Publications: New York, 1993. (b) *Magneto-Structural Correlations in Exchange Coupled Systems*; Willet, R. D., Gatteschi, D., Kahn, O., Eds.; Reidel: Dordrecht, The Netherlands, 1985. (c) *Research Frontiers in Magnetochemistry*; O'Connor, C. J., Ed.; World Scientific: Singapore, 1993. (d) Ribas, J.; Escuer, A.; Monfort, M.; Vicente, R.; Cortés, R.; Lezama, L.; Rojo, T. *Coord. Chem. Rev.* **1999**, *193*−*195*, 1027–1068.

(2) (a) Thompson, L. K.; Mandal, S. K.; Tandon, S. S.; Bridson, J. N.; Park, M. K. *Inorg. Chem.* **1996**, *35*, 3117–3125. (b) Nanda, K. K.; Thompson, L. K.; Bridson, J. N.; Nag, K. *J. Chem. Soc., Chem. Commun.* **1994**, 1337–1338. (c) Mohanta, S.; Nanda, K. K.; Thompson, L. K.; Flörke, U.; Nag, K. *Inorg. Chem.* **1998**, *37*, 1465–1472. (d) Koner, R.; Hazra, S.; Fleck, M.; Jana, A.; Lucas, C. R.; Mohanta, S. *Eur. J. Inorg. Chem.* **2009**, 4982–4988. (e) Chaudhuri, P.; Wagner, R.; Khanra, S.; Weyhermuller, T. *Dalton Trans.* **2006**, 4962–4968.

(3) (a) Sasmal, S.; Hazra, S.; Kundu, P.; Majumder, S.; Aliaga-Alcalde, N.; Ruiz, E.; Mohanta, S. *Inorg. Chem.* **2010**, *49*, 9517–9526. (b) Palacios, M. A.; Mota, A. J.; Perea-Buceta, J. E.; White, F. J.; Brechin, E. K.; Colacio, E. *Inorg. Chem.* **2010**, *49*, 10156–10165. (c) Halcrow, M. A.; Sun, J. S.; Huffman, J. C.; Christou, G. *Inorg. Chem.* **1995**, *34*, 4167–4177.

(4) (a) Ruiz, E.; Cano, J.; Alvarez, S.; Alemany, P. *J. Am. Chem. Soc.* **1998**, *120*, 11122–11129. (b) Ruiz, E.; Alemany, P.; Alvarez, S.; Cano, J. *J. Am. Chem. Soc.* **1997**, *119*, 1297–1303. (c) Cauchy, T.; Ruiz, E.; Alvarez, S. *J. Am. Chem. Soc.* **2006**, *128*, 15722–15727. (d) Rajaraman, G.; Totti, F.; Bencini, A.; Caneschi, A.; Sessoli, R.; Gatteschi, D. *Dalton Trans.* **2009**, 3153–3161. (e) Manca, G.; Cano, J.; Ruiz, E. *Inorg. Chem.* **2009**, *48*, 3139–3144. (f) Triki, S.; Gómez-García, C. J.; Ruiz, E.; Sala-Pala, J. *Inorg. Chem.* **2005**, *45*, 5501–5508.

(5) (a) *Single-Molecule Magnets and Related Phenomena*; Winpenny, R., Ed.; Springer: New York, 2006. (b) *Extended Linear Chain Compounds*; Miller, J. S., Ed.; Plenum: New York, 1983; Vol. III. (c) *Magnetic Molecular Materials*; Gatteschi, D., Kahn, O., Miller, J. S., Palacio, F., Eds.; Kluwer Academic Publishers: Dordrecht, 1991. (d) *Magnetism: Molecules to Materials II*; Miller, J. S., Drillon, M., Eds.; Willey-VCH: Weinheim, 2001.

(6) (a) Lin, P.-H.; Burchell, T. J.; Ungur, L.; Chibotaru, L. F.; Wernsdorfer, W.; Murugesu, M. *Angew. Chem., Int. Ed.* **2009**, *48*, 9489–9492. (b) Freedman, D. E.; Jenkins, D. M.; Iavarone, A. T.; Long, J. R. *J. Am. Chem. Soc.* **2008**, *130*, 2884–2885. (c) Yoshihara, D.; Karasawa, S.; Koga, N. *J. Am. Chem. Soc.* **2008**, *130*, 10460–10461. (d) Ohkoshi, S.-i.; Ikeda, S.; Hozumi, T.; Kashiwagi, T.; Hashimoto, K. *J. Am. Chem. Soc.* **2006**, *128*, 5320–5321. (e) Vallejo, J.; Castro, I.; Ferrando-Soria, J.; Déniz-Hernández, M. d. P.; Ruiz-Pérez, C.; Lloret, F.; Julve, M.; Ruiz-García, R.; Cano, J. *Inorg. Chem.* **2011**, *50*, 2073–2075. (f) Sanchiz, J.; Pasán, J.; Fabelo, O.; Lloret, F.; Julve, M.; Ruiz-Pérez, C. *Inorg. Chem.* **2010**, *49*, 7880–7889.

(7) (a) Sessoli, R.; Gatteschi, D.; Caneschi, A.; Novak, M. A. *Nature* **1993**, *365*, 141–143. (b) Berlinguette, C. P.; Vaughn, D.; Cañada-Vilalta, C.; Galán-Mascarós, J. R.; Dunbar, K. R. *Angew. Chem., Int. Ed.* **2003**, *42*, 1523–1526. (c) Lampropoulos, C.; Redler, G.; Data, S.; Abboud, K. A.; Hill, S.; Christou, G. *Inorg. Chem.* **2010**, *49*, 1325–1336.

(8) (a) Chou, Y.-C.; Huang, S.-F.; Koner, R.; Lee, G.-H.; Wang, Y.; Mohanta, S.; Wei, H.-H. *Inorg. Chem.* **2004**, *43*, 2759–2761. (b) McKee, V.; Dagdigian, J. V.; Bau, R.; Reed, C. A. *J. Am. Chem. Soc.* **1981**, *103*, 7000–7001. (c) Mazurek, W.; Kennedy, B. J.; Murray, K. S.; O'Connor, M. J.; Rodgers, J. R.; Snow, M. R.; Wedd, A. G.; Zwack, P. R. *Inorg. Chem.* **1985**, *24*, 3258–3264. (d) Nishida, Y.; Kida, S. *J. Chem. Soc., Dalton Trans.* **1986**, 2633–2640. (e) Doman, T. N.; Williams, D. E.; Banks, J. F.; Buchanan, R. M.; Chang, H.-R.; Webb, R. J.; Hendrickson, D. N. *Inorg. Chem.* **1990**, *29*, 1058–1062.

(9) Hazra, S.; Koner, R.; Lemoine, P.; Sañudo, E. C.; Mohanta, S. *Eur. J. Inorg. Chem.* **2009**, 3458–3466.

(10) (a) Dey, S. K.; Mondal, N.; Fallah, M. S. E.; Vicente, R.; Escuer, A.; Solans, X.; Font-Bardía, M.; Matsushita, T.; Gramlich, V.; Mitra, S. *Inorg. Chem.* **2004**, *43*, 2427–2434. (b) Banerjee, A.; Singh, R.; Chopra, D.; Colacio, E.; Rajak, K. K. *Dalton Trans.* **2008**, 6539–6545.

(11) Roth, A.; Buchholz, A.; Rudolph, M.; Schütze, E.; Kothe, E.; Plass, W. *Chem.—Eur. J.* **2008**, *14*, 1571–1583.

(12) (a) Sato, T.; Mori, W.; Xie, Y.; Kanehisa, N.; Kai, Y.; Fuji, M.; Goto, S.; Nagai, E.; Nakao, Y. *Inorg. Chim. Acta* **2006**, *359*, 2271–2274. (b) Ambrosi, G.; Dapporto, P.; Formica, M.; Fusi, V.; Giorgi, L.; Guerri, A.; Micheloni, M.; Paoli, P.; Pontellini, R.; Rossi, P. *Dalton Trans.* **2004**, 3468–3474. (c) Boudalis, A. K.; Clemente-Juan, J.-M.; Dahan, F.; Tuchagues, J.-P. *Inorg. Chem.* **2004**, *43*, 1574–1586.

(13) (a) Bouwman, R.; Evans, P.; de Graaf, R. A. G.; Kooijman, H.; Poinsot, R.; Rabu, P.; Reedijk, J.; Spek, A. L. *Inorg. Chem.* **1995**, *34*, 6302–6311. (b) Clemente-Juan, J. M.; Mackiewicz, C.; Verelst, M.; Dahan, F.; Bousseksou, A.; Sanakis, Y.; Tuchagues, J.-P. *Inorg. Chem.* **2002**, *41*, 1478–1491. (c) Barandika, M. G.; Serna, Z.; Cortés, R.; Lezama, L.; Rojo, T.; Urtiaga, M. K.; Arriortua, M. I. *Chem. Commun.* **2001**, 45–46.

(14) (a) Aromí, G.; Parsons, S.; Wernsdorfer, W.; Brechin, E. K.; McInnes, E. J. L. *Chem. Commun.* **2005**, 5038–5040. (b) Stamatatos, T. C.; Abboud, K. A.; Perlepes, S. P.; Christou, G. *Dalton Trans.* **2007**, 3861–3863.

(15) (a) Tong, M.-L.; Monfort, M.; Juan, J. M. C.; Chen, X.-M.; Bu, X.-H.; Ohba, M.; Kitagawa, S. *Chem. Commun.* **2005**, 233–235. (b) Wu, D.-Y.; Huang, W.; Hua, W.-J.; Song, Y.; Duan, C.-Y.; Li, S.-H.; Meng, Q.-J. *Dalton Trans.* **2007**, 1838–1845. (c) Serna, Z. E.; Lezama, L.; Urtiaga, M. K.; Arriortua, M. I.; Barandika, M. G.; Cortés, R.; Rojo, T. *Angew. Chem., Int. Ed.* **2000**, *39*, 344–347. (d) Serna, Z. E.; Barandika, M. G.; Cortés, R.; Urtiaga, M. K.; Barberis, G. E.; Rojo, T. *J. Chem. Soc., Dalton Trans.* **2000**, 29–34. (e) Ribas, J.; Monfort, M.; Costa, R.; Solans, X. *Inorg. Chem.* **1993**, *32*, 695–699. (f) Georgopoulou, A. N.; Raptopoulou, C. P.; Ballesteros, V. P. R.; Abarca, B.; Boudalis, A. K. *Inorg. Chem.* **2009**, *48*, 3167–3176.

(16) (a) Boeer, A. B.; Barra, A.-L.; Chibotaru, L. F.; Collision, D.; McInnes, E. J. L.; Mole, R. A.; Simeoni, G. G.; Timco, G. A.; Ungur, L.; Unruh, T.; Winpenny, R. E. P. *Angew. Chem., Int. Ed.* **2011**, *50*, 4007–4011. (b) Chibotaru, L. F.; Ungur, L.; Aronica, C.; Elmoll, H.; Pilet, G.; Luneau, D. *J. Am. Chem. Soc.* **2008**, *130*, 12445–12455. (c) Hendrickx, M. F. A.; Clima, S.; Chibotaru, L. F.; Ceulemans, A. *J. Phys. Chem. A* **2005**, *109*, 8857–8864. (d) Ceulemans, A.; Chibotaru, L. F.; Heylen, G. A.; Pierloot, K.; Vanquickenborne, L. G. *Chem. Rev.* **2000**, *100*, 787–806. (e) Van den Heuvel, W.; Chibotaru, L. F. *Inorg. Chem.* **2009**, *48*, 7557–7563.

(17) (a) Ruiz, E.; Alvarez, S.; Rodríguez-Fortea, A.; Alemany, P.; Pouillon, Y.; Massobrio, C. In *Magnetism: Molecules to Materials*; Miller, J. S., Drillon, M., Eds.; Wiley-VCH: Weinheim, 2001; Vol. 2, p 227. (b) Desplanches, C.; Ruiz, E.; Rodríguez-Fortea, A.; Alvarez, S. *J. Am. Chem. Soc.* **2002**, *124*, 5197–5205. (c) Cremades, E.; Ruiz, E. *Inorg. Chem.* **2010**, *49*, 9641–9648. (d) Ruiz, E.; Cauchy, T.; Cano, J.; Costa, R.; Tercero, J.; Alvarez, S. *J. Am. Chem. Soc.* **2008**, *130*, 7420–7426.

(18) (a) Ruiz, E.; Cano, J.; Alvarez, S.; Caneschi, A.; Gatteschi, D. *J. Am. Chem. Soc.* **2003**, *152*, 6791–6794. (b) Rajaraman, G.; Cano, J.; Brechin, E. K.; McInnes, E. J. L. *Chem. Commun.* **2004**, 1476–1477. (c) Christian, P.; Rajaraman, G.; Harrison, A.; McDouall, J. J. W.; Raftery, J.; Winpenny, R. E. P. *Dalton. Trans.* **2004**, 2550–2555. (d) Rajaraman, G.; Murugesu, M.; Sañudo, E. C.; Soler, M.; Wernsdorfer, W.; Helliwell, M.; Muryn, C.; Raftery, J.; Teat, S. J.; Christou, G.; Brechin, E. K. *J. Am. Chem. Soc.* **2004**, *126*, 15445–15457. (e) Hegetschweiler, K.; Morenstern, B.; Zubieta, J.; Hagrman, P. J.; Lima, N.; Sessoli, R.; Totti, F. *Angew. Chem., Int. Ed.* **2004**, *43*, 3436–3439.

(19) (a) Suaud, N.; Bolvin, H.; Daudey, J. *Inorg. Chem.* **1999**, *38*, 6089–6095. (b) Monari, A.; Maynau, D.; Malrieu, J.-P. *J. Chem. Phys.* **2010**, *133*, 044106(1)–044106(11).

(20) Noodleman, L. *J. Chem. Phys.* **1981**, *74*, 5737–5743.

(21) Ruiz, E.; Alvarez, S.; Cano, J.; Alemany, P. *J. Comput. Chem.* **1999**, *20*, 1391–1400.

(22) (a) Ruiz, E.; Rodríguez-Fortea, A.; Cano, J.; Alvarez, S.; Alemany, P. *J. Comput. Chem.* **2003**, *24*, 982–989. (b) Bencini, A.; Totti, F. *Int. J. Quantum Chem.* **2005**, *101*, 819–825.

(23) Becke, A. D. *J. Chem. Phys.* **1993**, *98*, 5648–5652.

(24) (a) Schäfer, A.; Horn, H.; Ahlrichs, R. *J. Chem. Phys.* **1992**, *97*, 2571–2577. (b) Schäfer, A.; Huber, C.; Ahlrichs, R. *J. Chem. Phys.* **1994**, *100*, 5829–5835.

(25) Frisch, M. J.; et al. *Gaussian 03*, Revision C.1; Gaussian, Inc.: Pittsburgh, PA, 2003.

(26) (a) *APEX-II, SAINT-Plus, and TWINABS*; Bruker-Nonius AXS, Inc.: Madison, WI, 2004. (b) Sheldrick, G. M. *SAINT*, Version 6.02, *SADABS*, Version 2.03; Bruker AXS, lnc.: Madison, WI, 2002. (c) *SHELXTL*, version 6.10; Bruker AXS Inc.: Madison, WI, 2002. (d) Sheldrick, G. M. *SHELXL-97, Crystal Structure Refinement Program*; University of Göttingen: Göttingen, 1997.

(27) It may be noted that the theoretical saturation value of magnetization for a $S = 2$ state with $g = 2.25$ and with no single-ion anisotropy should be 4.5 μ_B, and therefore the slightly smaller value, 4 μ_B, indicates the presence of low-lying excited states and anisotropy.

(28) Borrás-Almenar, J. J.; Clemente-Juan, J. M.; Coronado, E.; Tsukerblat, B. S. *Inorg. Chem.* **1999**, *38*, 6081–6088.

(29) Kahn, O.; Briat, B. *J. Chem. Soc., Faraday Trans. 2* **1976**, *72*, 268–281.